Research Square

Preprints are preliminary reports that have not undergone peer review.
They should not be considered conclusive, used to inform clinical practice,
or referenced by the media as validated information.

Pristane induced lupus mice as a model for neuropsychiatric lupus (NPSLE)

Yang Yun
Shengjing Hospital of China Medical University, Department of Nephrology
Xuejiao Wang
China Medical University, Department of Physiology
Jingyi Xu
First Affiliated Hospital of China Medical Universtiy, Department of Rheumatology and Immunology
Chenye Jin
First Affiliated Hospital of China Medical Universtiy, Department of Rheumatology and Immunology
Jingyu Chen
China Medical University, Department of Physiology
Xueru Wang
China Medical University, Department of Physiology
Jianing Wang
First Affiliated Hospital of China Medical Universtiy, Department of Rheumatology and Immunology
Ling Qin
China Medical University, Department of Physiology
Pingting Yang (yangpingtingting@163.com)
First Affiliated Hospital of China Medical Universtiy, Department of Rheumatology and Immunology

Research Article

Keywords: neuropsychiatric lupus, mouse model, behavioral deficit, cytokine, IgG, glia cells, lipofuscin

Posted Date: July 19th, 2022

DOI: https://doi.org/10.21203/rs.3.rs-1842109/v1

License: This work is licensed under a Creative Commons Attribution 4.0 International License.
Read Full License

Additional Declarations: No competing interests reported.

Version of Record: A version of this preprint was published at Behavioral and Brain Functions on February 10th, 2023. See the published version at https://doi.org/10.1186/s12993-023-00205-y.

Abstract

Background

Pristane induced lupus (PIL) model is a useful tool to study environmental-related systemic lupus erythematosus (SLE). However, the involvement of neuropsychiatric manifestations in this model has not been investigated in detail. Since neuropsychiatric lupus (NPSLE) is an important complication of SLE, we investigated how PIL mice develop neuropsychiatric symptoms to explore its suitability for NPSLE study.

Results

We found that PIL mice showed olfactory dysfunction accompanied with an anxiety- and depression-like phenotype at month 2 or 4 after pristane injection. The levels of cytokines (IL-1β, IL-6, TNF-α and IL-10) in the brain and BBB permeability increased significantly from month 1, and persisted throughout the observed course of the disease. Then, IgG deposition in the choroid plexus and lateral ventricle wall were observed at month 1. Both astrocytes and microglia were activated at month 1. The activation of astrocytes was persistent throughout the observed course of the disease, while the microglia activation decayed dramatically at month 4. Lipofuscin deposition, a sign of neuronal damage, was detected in cortical and hippocampal neurons from month 4 to 8.

Conclusion

PIL mice showed a series of behavioral deficits and pathological changes in the brain, which might be applicable to investigate the development of pathogenesis and potential therapeutic targets of environmental-related NPSLE.

1. Background

Systemic lupus erythematosus (SLE) is an intractable, multisystemic and relapsing disease characterized primarily by the loss of tolerance to self-antigens, immune complex formation and diverse end-organ damages[1]. Nervous system involvement in SLE affecting cognition, mood and the level of consciousness is called neuropsychiatric lupus (NPSLE), which is associated with worse prognosis and more cumulative organ damage[2, 3]. As for the pathogenesis of NPSLE, it is generally believed that several pathogenic factors, such as autoantibodies, immune cells and inflammatory mediators, may disrupt the blood-brain barrier (BBB) and promote an inflammatory process causing glial activation, neurodegeneration and behavioral deficits[4–6]. However, the detailed mechanism of NPSLE remains largely unknown.

Human research on NPSLE is limited by the difficulty to perform brain biopsy. Although histological analysis can be conducted on autopsy, rapid decomposition of brain tissue seriously impact on the results. Therefore, animal models of NPSLE are indispensable tools for exploration of the pathogenic mechanisms[7]. MRL/lpr and NZB/W F1 mice are commonly used as NPSLE animal models, which spontaneously develop neuropsychiatric symptoms such as cognitive dysfunction[8, 9], anxiety and/or depression-like behavior[8, 10, 11] and decreased locomotor activity[12]. However, these models rely on inbred mouse strains, exhibit delayed and inconsistent onset of SLE-related symptoms and progress slowly[13]. The heterogeneous and mild neuropsychiatric symptoms limit the application of these models on NPSLE research. Additionally, the role of environmental factors on the pathogenesis of NPSLE can not be fully reflected by these genetically predisposed models.

Applying chemical agents to wild-type mice is another method to establish a SLE model, which can mimic the effects of environmental factors to induce lupus-specific manifestations. Such a model enables to investigate non-genetic factors initiating a breakdown of immune tolerance and evaluate the efficacy of SLE therapeutic drugs. Pristane is known as hydrocarbon oil (2, 6, 10, 14-tetramethylpentadecane) that can induce a wide range of autoantibodies specific to or associated with SLE in mice. In nature, this oil can be found in small amounts in vegetables[14], in the liver of some sharks[15], and as a byproduct of petroleum distillation[14]. Administration of pristane into the abdominal cavity of mice can cause a serial of lupus-like manifestations, including ascitic fluid enriched with monoclonal antibodies, lipogranulomas, rheumatoid-like erosive arthritis and diffuse proliferative glomerulonephritis[16]. Though most of the major clinical and laboratory manifestations of SLE well described by the American College of Rheumatology have been observed in the pristane induced lupus (PIL) model, there are few reports about NPSLE manifestations in this model[17–19]. For this, we combined behavioral, histomorphological and biochemical approaches to comprehensively evaluate brain dysfunctions and pathological changes in the PIL model. Our findings highlight the significance of the PIL model on the research of cellular and molecular mechanisms underlying environmental-related NPSLE.

2. Results

2.1 Lupus-like manifestations of PIL mice

Consistent with previous studies[18, 20, 21], PIL mice in our study presented several representative lupus-like manifestations, including lipogranuloma, elevated serum cytokines and autoantibodies, immune complex mediated nephritis, arthritis, as well as splenomegaly (Fig. 2). Lipogranuloma adherent to the abdominal surface of the diaphragm appeared at month 1 after pristane injection, and progressed over time (Fig. 2A). Meanwhile, the serum levels of cytokines (IL-1β, IL-6, TNF-α and IL-10), total IgG and anti-dsDNA in PIL mice increased higher than those in their age matched controls from month 1 or 2 (Fig. 2B; $p < 0.05$, $p < 0.01$). Granular deposits of IgG (Fig. 2C) and C3 (Fig. 2D) were also observed in the glomeruli of PIL mice. The MFI of IgG and C3 increased significantly at month 2, and further increased with time (Fig. 2C-

D; $p < 0.05$, $p < 0.01$). At month 4, symmetrical swelling appeared in the hind paws of PIL mice (Fig. 2E). Compared with control mice, arthritis severity score showed a significant elevation in PIL mice from month 4 to 8 (Fig. 2E; $p < 0.05$, $p < 0.01$). Splenomegaly was observed in PIL mice, and the increase of spleen index became significantly at month 8 (Fig. 2F; $p < 0.01$). Taken together, PIL mice represented typical lupus-like manifestations during the observed course of the disease.

2.2 PIL mice displayed olfactory dysfunction and an anxiety- and depression-like phenotype

We used a battery of behavioral tests to assess the neuropsychiatric phenotype of PIL mice. As shown in Fig. 3A, PIL mice spent less time sniffing male or female fecal dilute solution than their age matched controls from month 2 ($p < 0.05$, $p < 0.01$). Although not statistically significant, a trend toward the increase of time spent sniffing vinegar and alcohol was also observed in PIL mice (Fig. 3A; $p > 0.05$). These results indicated that PIL mice lost their interest in attractants, especially biological odorants, and decreased sensitivity to repellants.In the open field test, both the total track distance and time spent in center decreased with time in PIL mice, and the significant difference between PIL and control mice appeared at month 4 (Fig. 3B; $p < 0.05$, $p < 0.01$). Consistent with the results in open field test, PIL mice exhibited anxiety-like behavior in the elevated zero maze test as evidenced by significantly decreased total track distance and time spent in open arms from month 4, and further decreased with time (Fig. 3C; $p < 0.05$, $p < 0.01$). Furthermore, immobility time of PIL mice significantly increased in the forced swim test from month 4 to 8 (Fig. 3D; $p < 0.05$, $p < 0.01$). There were no differences between PIL mice and their age matched controls in novel object recognition test, social novelty preference test, rotarod test or PPI test at any testing time point (Fig. 4). Therefore, the olfactory function of PIL mice was impaired earlier, while the anxiety- and depression- like phenotype appeared later.

2.3 Overproduction of brain cytokines and BBB leakage in PIL mice

ELISA assays revealed that the levels of IL-1β, IL-6, TNF-α and IL-10 were elevated significantly in the brain tissues of PIL mice as compared with their age matched controls at month 1, and maintained throughout the observed course of the disease (Fig. 5A; $p < 0.01$). Although no obvious pathological changes, such as parenchymal lesions, ischemic lesions by vasculitis or thromboembolism, and brain atrophy, were observed in the brain of PIL mice (data not shown), BBB permeability determined by evaluating the extravasation of evans blue showed some abnormalities. Compared with age-matched controls, there was a marked increase in evans blue content in the brain of PIL mice at month 1 and maintained relatively stable throughout the observed course of the disease (Fig. 5B; $p < 0.05$, $p < 0.01$).

2.4 IgG deposition in the brain of PIL mice

Immunofluorescence staining of the brain sections showed that IgG deposition appeared in the choroid plexus and lateral ventricular wall of PIL mice at month 1 and gradually increased with the progress of the disease (Fig. 6; $p < 0.01$). Some IgGs co-localized with microglia (stained by Iba-1) in PIL mice (Fig. 6A,

B). Since there is no difference of IgG deposition between age-matched controls at any testing time point, we showed the representative images of control (1m) group in Fig. 6A and B for brevity.

2.5. Dynamic changes of microglia and astrocytes in the hippocampus of PIL mice

Because hippocampus plays a critical role in olfactory function[22] and mood regulation[23], our results of behavioral tests suggest an involvement of hippocampus in PIL mice. We then conducted immunohistochemical staining on the brain slices to examine the effects of pristane injection on glia cells of hippocampus. We gauged and compared the distribution of cells immunoreactive for microglial marker (Iba-1) in the hippocampus. Compared with control mice, the density of Iba-1-immunoreactive microglia increased significantly in PIL mice at month 1, reached a peak at month 2, and then declined sharply (Fig. 7A, C; $p < 0.01$). Meanwhile, microglia in PIL mice showed a phenotypic transformation from ramified to an activated state characterized by bearing retracted processes and large irregular cell soma (Fig. 7A). Immunofluorescence staining also revealed that the density of GFAP-immunoreactive astrocytes significantly increased in the hippocampus of PIL mice at month 1 and maintained throughout the observed disease course (Fig. 7B, D; $p < 0.01$), accompanied with an activated morphological change of astrocytes (Fig. 7B). These results suggest that behavioral deficits of PIL mice were accompanied by dynamic changes of microglia and astrocytes.

2.6. Lipofuscin deposition in the brain of PIL mice

Lipofuscin, also called as “age-pigment”, is frequently found to aggregate in neurons of the subjects with neurodegenerative disorders, due to accumulation of oxidized cross-linked proteins, lipids and sugars in lysosomes of post-mitotic cells. Compared with age-matched control mice, we also found a significant increase of autofluorescent lipofuscin depositing in the cortex and hippocampus of PIL mice at month 4, and further increased with time (Fig. 8; $p < 0.01$). However, the density of NeuN-immunoreactive neurons in the cortex and hippocampus was not significantly different between PIL and control mice (data not shown). Furthermore, the TUNEL assay did not reveal a significant sign of apoptosis in both PIL and control mice (data not shown). But this can not completely exclude the possibility of apoptosis in PIL mice, as TUNEL assay only detects excessive apoptosis in vivo. More systemic experiments are warranted to fully examine whether neuronal apoptosis is existed in PIL mice.

3. Discussion

To best represent human disease, and explore relevant pathogenesis and novel treatment approaches, it is crucial to take full advantage of the available mouse models of spontaneous or inducible lupus-like disease. However, previous studies prefer using genetically susceptible animals to investigate spontaneous NPSLE[24]. Neuropsychiatric symptoms in the inducible wild-type models of lupus are less studied. Here, we systematically evaluated whether PIL mice are possible to be used as an environmental-related inducible model of NPSLE. Consistent with previous reports[18, 20, 21], we verified PIL mice presenting several peripheral lupus-like manifestations (Fig. 2). We further revealed some brain

dysfunctions and neuropathological changes: a) olfactory dysfunction and an anxiety- and depression-like phenotype. b) cytokine overproduction in the brain tissues. c) BBB leakage. d) IgG deposition in the choroid plexus and lateral ventricular wall, and co-localization of IgG with microglia. e) changes of morphology and density of microglia and astrocytes in the hippocampus. f) lipofuscin deposition in the cortical and hippocampal neurons. Our results highlight the potential application of PIL mice for exploring the pathogenesis of environmental-related NPSLE.

Many NPSLE patients usually have olfactory dysfunction[25]. Spontaneous lupus-prone MRL/lpr mice also displayed a constellation of behavioral deficits dependent on olfaction[26, 27]. In our study, PIL mice lost their interest in biological odorants, decreased sensitivity to repellents (Fig. 3A). And, these olfactory dysfunctions appeared earlier than other behavioral deficits, suggesting that olfactory neural system is highly sensitive to immune attack. Thus, olfactory function test might be an effective approach for early diagnosis of NPSLE. Additionally, affective deficits are frequent neuropsychiatric events in NPSLE[28], which impact on patients' health-related quality of life. Similarly, numerous genetically predisposed mouse models of NPSLE also exhibit affective disorders. For example, the MRL/lpr strain presents depression-like behavior and deficits in cognitive function without anxiety-like behavior[8]; NZB/W F1 mice exhibit congenital abnormalities, anxiety-like behavior and decreased locomotor activity[12] and B6.Nba2 mice show a strong anxiety phenotype and a mild depression phenotype[29]. Recently, several neuropsychiatric manifestations are also reported in PIL mice, including learning and memory disturbance[17] and decreased spontaneous activities[18]. In this study, we observed a severe and consistent anxiety- and depression- like phenotype in PIL mice from month 4 to 8 (Fig. 3B-D). In line with previous findings[30, 31], our results confirmed an association between olfactory dysfunction and depression-like behavior. However, no significant result was found in novel object recognition test, social novelty preference test, rotarod test and PPI test (Fig. 4). It should be noted that the MRL background of MRL/lpr mice itself may be involved in the severity of neurobehavioral abnormalities[24]. Whereas, our PIL mice, without specific genetic background, are more suitable to investigate the neuroimmune mechanism of NPSLE.

Several observations have suggested that cytokine dysregulation may contribute to depression-like behavior of NPSLE. First, increased levels of cytokines, especially IL-6, IL-8, IL-1, TNF-α and interferon-α (IFN-α), are found in the cerebrospinal fluid of NPSLE patients[32–35]. Second, the early dysregulation of cytokine production concords with the onset of symptoms of depressive-like behavior in MRL/lpr mice[36] and in other rodent strains[37, 38]. Third, anhedonia and other behavioral indices of depressive-like behavior in mice can be replicated by exogenous cytokines, such as IL-6 and TNFα[36, 39], and are prevented by knockout of their receptors[39, 40]. In this study, we found substantial increase of cytokine expression (IL-1β, IL-6, TNF-α and IL-10) in the brain of PIL mice at as early as month 1 (Fig. 5A). Because cytokine overexpression occurred earlier than behavioral deficits, it may be one of the initiating factors in the depressive-like behavior of PIL mice. The increase of cytokine levels in the brain might be attributable to an interaction between the peripheral and central immune systems. Pristane, known as a membrane-

activating compound, can induce apoptosis in peripheral tissues, and produces sufficient autoantigen substrates for immune intolerance, which can lead to overproduction of cytokines and development of lupus-like autoimmunity[41]. The increased peripheral inflammatory cytokines can enter into the brain directly[42] or disrupt the integrity of BBB[43, 44] by acting on vascular endothelial cells[45–47]. In this study, we detected significant extravasation of evens blue dye in the brain tissues suggesting a leakage of BBB in PIL mice (Fig. 5B). Meanwhile, the innate immune cells in the brain, such as glia cells, can be activated and produce more inflammatory cytokines. Previous studies on the models with systemic inflammation have revealed an increase of glia activation even under the condition of intact BBB[48]. Furthermore, we found IgG deposition in the choroid plexus and lateral ventricular wall (Fig. 6). A significant increase of IgG deposition has also been observed in the hippocampus zone of PIL mice[19]. IgG deposition in the brain may occur following the impairment of blood ventricular barrier and choroid plexus vascular barrier caused by cytokines in PIL mice. IgG deposition can promote endothelial damage, microglial activation and inflammatory mediator production, resulting in a positive feedback loop to disrupt the balance of immunity homeostasis[49, 50]. Furthermore, we found an indication of phagocytosis of IgG by microglia (co-localization of IgG with microglia), suggesting that microglia may play a neuroprotective role in PIL mice.

Microglia are innate immune cells in the brain, connecting the nervous system with the immune system. Several studies have suggested that microglia are involved in the development of neuropsychiatric symptoms of NPSLE. First, microglia can be activated by cytokines, such as TNF-α, and inhibited by downregulating markers of microglia activation in MRL/lpr mice[51]. Second, microglia may initially migrate to BBB to protect its integrity, and then transform into a reactive phenotype to destroy BBB and trigger neuroinflammation in NPSLE model mice[52]. Third, antagonism of microglia activation can significantly attenuate spatial memory deficit and depression-like behavior in MRL/lpr mice[53]. In line with these, we found microglial activation during the initial stage of the disease in PIL mice, indicated by an increase of microglia density and specific morphological changes (Fig. 7A, C). It has been suggested that activated microglia may play a neuroprotective role during the early stage of neurodegenerative disorders[54]. Microglia could respond to the stimulation of neurotransmitters, such as adenosine triphosphate (ATP), glutamate and histamine, released by damaged neurons, and consequently enhance phagocytic activity to clear unwanted debris, protein aggregates and soluble antigens, thus reduce their damaging effects on neurons[55]. However, we also found the density of microglia declined sharply in the hippocampus of PIL mice from month 4 to 8. The sustained immune attack during the protracted process of SLE may cause activation-mediated apoptosis of microglia[56]. The loss of microglia may severely hamper their capacity for combating immune challenge and repairing tissues, resulting in neural damages and behavioral deficits. It is noted that recent study has demonstrated that the neuronal degeneration or remodeling induced by the interaction between activated microglia and neurons may contribute to the cognitive dysfunction[57]. One limitation of our study was lack of the examination of neuronal degeneration markers, such as neuronal complexity, length of dendrites and the number of spines in the brain of PIL mice. This issue is required to be fully investigated in the future. Together with

previous results, our findings suggest that the dynamic change of microglia is an important involvement of the neuropathology of NPSLE, and regulating microglia may be a promising therapeutic strategy for NPSLE. In contrast, astrocytes were persistently activated throughout the observed course of the disease in PIL mice (Fig. 7B, D). Astrocytes generally interact with both neural and non-neural cells and exhibit dynamic activities crucial for neural circuit function, neurological function and behavior[58]. In neural disorders, astrocytes can be activated and produce nerve growth factors and immune mediators, such as IL-1 and nitric oxide (NO), in response to brain inflammation or injury[59]. Histopathological investigations of NPSLE patients' brains confirm the widespread presence of activated astrocytes along with microglia in the heterogeneous pathological changes[60]. As astrocytes are an important component of BBB, activated astrocytes are the typical hallmark of BBB dysfunction[61]. In addition to the physiological role of astrocytes in synaptic refinement, activated astrocytes have also been implicated in pathological synapse loss and dysfunction following injury or nervous system degeneration in adults[62]. Overall, astrocyte activation may contribute to the neural dysfunction in PIL mice, however the detailed mechanisms warrant further studies.

Another important finding of our study was that lipofuscin deposited in the neurons of both cortex and hippocampus in PIL mice (Fig. 8). Lipofuscin, known as age pigments, are autofluorescent lipopigments formed by lipids, metals and misfolded proteins, which are especially abundant in neural cells. Lipofuscin within the brain increase not only with age but also with pathological processes such as neuronal dysfunction and a repertoire of cellular alterations, including oxidative stress, proteasome, lysosomal and mitochondrial dysfunctions[63–67]. Recent evidence has suggested that lipofuscin may represent a risk factor or driver for different neurodegenerative disorders[68]. Furthermore, senescent neural cells have been found accumulating in the hippocampal of MRL/lpr SLE model mice with depressive behavior[69]. The increase of lipofuscin deposition in PIL mice may be attributable to the overexpression of cytokines in the brain, which can induce the synthesis of oxidative stress products. Accumulated oxidative stress products within neurons may orchestrate inflammation, disrupt the metabolisms of lipid and metals, and then promote the generation of lipofuscin. Loss of neuroprotective effects from microglia may accelerate this pathological process during the progressive stage of SLE. Even though, we neither observed significant changes of neuron density nor signs of neural apoptosis in the cortex and hippocampus. Thus, lipofuscin deposition is not a consequence of increased neuronal cell death and neural dysfunctions in PIL mice remain reversible.

4. Conclusions

In conclusions, we found that pristane can induce mice to exhibit olfactory dysfunction and an anxiety- and depression-like phenotype along with enhanced expression of cytokines, BBB leakage, activation of microglia and astrocytes and aberrant deposition of IgG and lipofuscin in the brain. Our results suggest that brain dysfunction of PIL mice may initiate from the dysregulation of cytokines, which subsequently triggers BBB impairment, IgG deposition, microglia activation and neuronal damage. These findings

suggest that PIL mice are a promising model for NPSLE study, and highlight the important roles of glia cells in the pathological mechanism of NPSLE, which may be a potential therapeutic target for NPSLE.

5. Methods

5.1. Animals

Specific pathogen-free BALB/c mice were purchased from the Vital River Laboratory (Beijing, CHN) at the age of 4 weeks. Female mice were used for the experiment at the age of 8 weeks. All animals were reared in standard animal cages under environmentally controlled laboratory conditions (12 h/12 h light/dark cycle, 22 ± 2°C, 40–80% humidity) with ad libitum access to food and water. All efforts were made to minimize animal suffering. The animals were maintained and treated in compliance with the policies and procedures detailed in the “Guide for the Care and Use of Laboratory Animals” of the National Institutes of Health. The Animal Care and Use Committee of China Medical University reviewed and approved the animal experimental protocols of the “Guide” and the treatment procedures (No. KT2018060).

5.2. Pristane injection

As shown in Fig. 1, at the age of 8 weeks, mice were randomly divided into the following eight groups (n = 12 in each group): 4 control groups (1m, 2m, 4m and 8m) and 4 PIL groups (1m, 2m, 4m and 8m), which received a single intraperitoneal injection of 0.5 ml phosphate buffer saline (PBS) or pristane (Sigma-Aldrich, St.Louis, MO, USA), respectively. The dose of pristane used in this study was based on a previous research[70]. Mice were sacrificed at month 1, 2, 4 or 8m after conducted a battery of behavioral tests. Blood samples were obtained from mouse eyeball. Tissue samples of spleen, kidney and brain were harvested for further examination. There was no early euthanasia of animal during the study.

5.3. ELISA for brain cytokines, and serum cytokines, total IgG and anti-dsDNA IgG detection

Mice were anesthetized and transcardially perfused with 0.1 M PBS (pH 7.5, 4°C). Brain tissue samples were harvested from mice and dissected into left and right hemispheres. One hemisphere was snap-frozen in liquid nitrogen and subsequently made into frozen sections for immunofluorescence staining, while the other hemisphere was homogenized on ice in PBS and centrifuged at 12,000 rpm for 15 min at 4°C to remove cell debris. Supernatants were collected and stored at -80°C until the measurement. Serum was separated via centrifugation at 5,000 rpm for 15 min at 4°C. Cytokines in brain tissues and serum were detected using mouse interleukin-1β (IL-1β), IL-6, tumor necrosis factors-α (TNF-α) and IL-10 ELISA kits (Boster & BiologicalTechnology, Wuhan, CHN). The levels of serum total immunoglobin G (IgG) and serum anti-double stranded DNA (anti-dsDNA) IgG were examined using an IgG ELISA kit (Boster & BiologicalTechnology, Wuhan, CHN) and an anti-dsDNA antibody ELISA kit (CUSABIO, Wuhan, CHN), respectively. Experimental procedures were strictly followed according to the manufacturer’s instructions. Absorbance at 450 nm was determined using a Bio-Rad Model 550 Microplate Reader (Berkeley, CA, USA). Each sample was tested at least three times, and the average value was taken.

5.4. Arthritis severity score

For quantified scoring of arthritis severity, we used a previously published scoring system[16], as follows: score scale of 0–3, where 0 = normal, 1 = slight swelling or erythema of the wrist/ankle joint or footpad, 2 = moderate swelling and erythema of the wrist/ankle joint or footpad, and 3 = severe swelling and erythema of the paw. The scores for individual limbs were summed to obtain a total arthritis severity score of 12 per animal. Arthritis severity score was assessed twice by two independent observers.

5.5. Spleen index

Spleen index of each mouse was calculated by the ratio of spleen weight to body weight (mg/g) as reported previously[18].

5.6. Behavioral assessments

The mice were subjected to a series of behavioral tests in the following order: olfactory sensitivity test, open field test, elevated plus maze test, novel object test, social novelty preference test, rotarod test, prepulse inhibition (PPI) test and forced swim test. Mice were tested during the same lighting and time-of-day conditions. All behavioral chambers were cleaned with 70% ethanol as changing mice. Researchers were blinded to experimental groups.

5.6.1. Olfactory sensitivity test

The paradigm used to assess olfactory sensitivity in this study was similar to an earlier report[27]. Following habituation to a new test chamber (45 cm × 24 cm × 20 cm), each mouse was introduced to a 5 cm × 5 cm piece of filter paper scented with 0.25 ml of an odorant for 2 min. Then, the scented filter paper was removed, and the mouse was allowed to rest for 1 min. The procedure mentioned above was repeated three times. Each mouse was presented with repellents (vinegar and alcohol) and attractants (male feces and female feces) diluted with PBS to the same concentration. Test chamber was covered with a clear piece of plexiglas to limit evaporation and entry of external odorants. Active investigation was defined as directed sniffing within 0.5 cm of the odorant source and the sniffing time was recorded. Sniffing time for each time was summed to obtain a total value per animal.

5.6.2. Open field test

Open field chamber (40 cm × 28 cm × 40 cm) was made up of black polyvinyl chloride (PVC) panels with a non-reflective base. The central zone was defined as a 20 cm × 14 cm area. Each mouse was positioned individually in the center zone and allowed to freely explore the arena for 30 min. Total distance travelled (km) and time spent in center (s) were digitally recorded and analyzed by custom-built programs.

5.6.3. Elevated zero maze test

The elevated zero maze was a ring-shaped apparatus, elevated 50 cm from the floor. This apparatus was consisted of a circular platform (outer diameter 50 cm, width 10 cm) divided into four quadrants of equal length with two open arms and two closed arms (surrounded by a 20-cm wall from the surface of the maze). The elevated zero maze test was conducted as previously described[71]. The test mouse was placed at the open arm and was allowed to conduct a 10-min free exploration. Total distance travelled (m) and percentage of time spent in the open arms were digitally recorded and analyzed by custom-built programs.

5.6.4. Novel object recognition test

The novel object recognition test was used to evaluate the recognition memory of mice and was conducted as previously described[72, 73]. During the acclimation phase, mice were allowed to habituate to the apparatus (55cm × 40cm × 30 cm) with no objects for 10 min, and then a test phase began 24 h later. On the trial day, two identical cylinder objects were placed in the opposite side of the apparatus, and mice were allowed to spend 10 min with the objects. One hour later, one of the objects was replaced with a triangular object, and time spent exploring the novel and familiar object were digitally recorded for 10 min. The time spent in close interaction with each object was converted into a discrimination ratio, which was calculated as follows: time spent exploring the novel object/total time spent exploring both objects.

5.6.5. Social novelty preference test

The social novelty preference test was performed as previously described, with minor modification[74, 75]. During the acclimation phase, a test mouse was allowed to habituate to the apparatus for 10 min. A stranger mouse was then placed in one of the wire cages. The test mouse was allowed to spend 10 min to explore the entire apparatus. Subsequently, a novel stranger mouse was placed in the other wire cage. The test mouse was allowed to freely investigate the entire apparatus (the familiar mouse in one corner and the novel stranger mouse in the opposite corner) for 10 min. The time spent in close interaction with each mouse was digitally recorded and converted into a discrimination ratio, which was calculated as follows: time spent exploring the stranger mouse/total time spent exploring both mice.

5.6.6. Rotarod test

The rotarod test was used to evaluate the motor coordination of mice and performed as previously described, with minor modification[18]. First, mice were placed on the stationary bar to habituate to the apparatus for 2 min. Then, mice were conducted to the rotarod test with accelerating speed from 4 to 40 rpm. Latency to fall off the rotating rod was recorded with a 5-min cutoff time for three trials per day over 3 consecutive days and the mean retention time on the rod per trail was recorded.

5.6.7. PPI test

PPI test was measured using a startle chamber and conducted as previously described, with minor modification[76, 77]. The test mouse was given a 10-min acclimation period in the startle chamber during which a 70 dB background noise was presented, and then the test mouse was subjected to test trials consisting of four trial types, that is, one type of startle stimulus only trial and three types of PPI trials.

White noise of 120 dB (40 ms) was used as the startle stimulus for all trial types. The peak startle amplitude was recorded with the onset of the startle sound. The prepulse stimulus was presented 100 ms before the onset of the startle stimulus, and its intensity was 75, 85 or 95 dB (20 ms). Six blocks of the four trial types were presented in a pseudorandom order such that each trial type was presented once within a block. The intertrial interval had an average duration of 15 sec. PPI responses were calculated as follows: PPI% = [1 − (prepulse trials/startle only trials)] × 100.

5.6.8. Forced swim test

Each mouse was placed into a glass beaker containing 3000 ml of water maintained at approximately 24 ± 1°C. Following habituation to swim in this glass breaker for 2 min, a 4-min test session was digitally recorded. Mice placed in this situation with no way to escape, and then began struggling and swimming but eventually exhibited behavioral despair, assessed as immobility[30]. Depression-like behavior was defined as immobility and was illustrated as the time spent immobile.

5.7. Measurement of BBB permeability

To evaluate alterations in BBB permeability, evans blue dye was used as a marker of BBB leakage, as previously described [78]. Briefly, mice received 2% evans blue dye solution (4 ml/kg, Beyotime biotechnology, Shanghai, CHN) intravenously 30 min before sacrifice. Then, the brain tissues were homogenized in 50% trichloroacetic acid at 1:3 volume ratios. BBB permeability was illustrated as evans blue extravasation, and was quantified in the supernatant from each sample following addition of 90 μl of 95% ethanol (absorbance, 620 nm).

5.8. Immunofluorescence staining

Kidney and brain tissues were dissected, fixed in 4% paraformaldehyde for 24 h, followed by 30% sucrose (w/v) solution at 4°C overnight, and utilized for frozen sections in a coronal plane. Then, 10-μm-thick frozen sections were cut, and blocked with 10% goat serum for 30 min at room temperature. Sections were incubated with primary antibodies of anti-complement 3 (C3) (1:100; Santa Cruz, CA, USA), anti-ionized calcium binding adapter molecule 1 (Iba-1) (1:200; Abcam, Cambridge, UK), anti-glial fibriliary acid protein (GFAP) (1:500; Abcam, Cambridge, UK) or anti-neuronal nuclei (NeuN) (1:500; Abcam, Cambridge, UK) at 4°C overnight. On the following day, sections were incubated with secondary antibodies of Alexa Fluor 488-conjugated goat anti-mouse IgG (1:200; Proteintech, Wuhan, CHN) or Alexa Fluor 488-conjugated goat anti-rabbit IgG (1:200, Proteintech, Wuhan, CHN) for 2 h at room temperature in the dark. For locating cell nuclei, sections were stained with DAPI (Beyotime biotechnology, Shanghai, CHN) for additional 8 min. Terminal deoxynucleotidyl transferase dUTP nick end labeling (TUNEL) staining was performed using a TUNEL Bright Green Apoptosis Detection kit (Vazyme, Nanjing, CHN) according to the manufacturer's instructions. Images were captured by a microscope (BX53, Olympus, JPN) at × 200 or × 400 magnification. The number of immunofluorescence stained cells was automatically counted in a defined area using Image J software. The mean fluorescent intensity (MFI) of C3 deposition in glomeruli was calculated using Image J software. The data from three random sections of each individual mouse were averaged to obtain a single value. For IgG staining, sections were

incubated with Alexa Fluor 594-conjugated goat anti-mouse IgG (1:200, Proteintech, Wuhan, CHN) for 2 hours at room temperature in the dark. The MFI of IgG deposition in choroid plexus, lateral ventricular wall or glomeruli was calculated using Image J software. To examine autofluorescent lipofuscin, regions of interest were captured at 480nm and 550nm exciting light. The mean gray value of autofluorescent lipofuscin was quantified by image J software.

5.9. Statistical analysis

GraphPad Prism V8 software (La Jolla, CA, USA) was used to perform statistical analysis. All data are expressed as the mean ± SEM. Differences were detected by repeated measures analysis of variance (ANOVA). The ANOVA reporting significant effects was followed by Tukey's post hoc test of multiple comparison. $P < 0.05$ was considered a statistically significant difference in all sampled groups.

Declarations

Authors' contributions

PTY and LQ supervised the project. PTY, LQ and YY designed the project, wrote the manuscript and performed the statistical analysis and revised the manuscript. YY, XJW, JYX and CYJ were involved in laboratory works and experimental design of the work. YY, JYC, XRW and JNW were involved in data collection and lab assessments, and study designing. All authors read and approved the final manuscript.

Funding

The study was funded by the Project for Construction of Key Platform, Shenyang, China (19-109-4-15 to PTY), "Xingliao Talent Plan" of Liaoning, China (XLYC2002062 to PTY), the Chinese National Key Technology R&D Program (2021YFC2501303 to PTY), the department of Science and Technology of Liaoning Province (2020JH2/10100014, 2021JH1/10400049 to LQ), the "Xingliao Talent Plan" of Liaoning, China (XLYC2002094 to LQ) and the fellowship of China Postdoctoral Science Foundation (2021M703606 to XJW).

Availability of data and materials

The data are available for any scientific use with kind permission.

Ethics approval and consent to participate

The animals were maintained and treated in compliance with the policies and procedures detailed in the "Guide for the Care and Use of Laboratory Animals" of the National Institutes of Health. The Animal Care and Use Committee of China Medical University reviewed and approved the animal experimental protocols of the "Guide" and the treatment procedures (No. KT2018060).

Consent for publication

Not applicable.

Competing interests

The authors declare that they have no competing interests.

Author details

[1]Department of Nephrology, Shengjing Hospital of China Medical University, Liaoning, 110004, China; [2] Department of Physiology, China Medical University, Liaoning, 110122, China; [3] Department of Rheumatology and Immunology, First Affiliated Hospital, China Medical University, Liaoning, 110001, China

References

1. Stock AD, Wen J, Doerner J, et al. Neuropsychiatric systemic lupus erythematosus persists despite attenuation of systemic disease in MRL/lpr mice. J Neuroinflammation. 2015; 12:205. https://doi.org/10.1186/s12974-015-0423-4.
2. Vivaldo JF, de Amorim JC, Julio PR, et al. Definition of NPSLE: Does the ACR Nomenclature Still Hold? Front Med (Lausanne). 2018; 5:138. https://doi.org/10.3389/fmed.2018.00138.
3. Popescu A, and Kao AH. Neuropsychiatric systemic lupus erythematosus. Curr Neuropharmacol. 2011; 9:449–57. https://doi.org/10.2174/157015911796557984.
4. Tomita M, Holman BJ, and Santoro TJ. Aberrant cytokine gene expression in the hippocampus in murine systemic lupus erythematosus. Neurosci Lett. 2001; 302:129 – 32. https://doi.org/10.1016/s0304-3940(01)01679-2.
5. Wen J, Stock AD, Chalmers SA, et al. The role of B cells and autoantibodies in neuropsychiatric lupus. Autoimmun Rev. 2016; 15:890–5. https://doi.org/10.1016/j.autrev.2016.07.009.
6. Daniel JW. Dubois' lupus erythematosus and related syndromes. St Louis, MO: Elsevier, 2018.
7. Vo A, Volpe BT, Tang CC, et al. Regional brain metabolism in a murine systemic lupus erythematosus model. J Cereb Blood Flow Metab. 2014; 34:1315–20. https://doi.org/10.1038/jcbfm.2014.85.
8. Li Y, Eskelund AR, Zhou H, et al. Behavioral Deficits Are Accompanied by Immunological and Neurochemical Changes in a Mouse Model for Neuropsychiatric Lupus (NP-SLE). Int J Mol Sci. 2015; 16:15150–71. https://doi.org/10.3390/ijms160715150.
9. Kier AB. Clinical neurology and brain histopathology in NZB/NZW F1 lupus mice. J Comp Pathol. 1990; 102:165 – 77. https://doi.org/10.1016/s0021-9975(08)80122-3.
10. Gao HX, Campbell SR, Cui MH, et al. Depression is an early disease manifestation in lupus-prone MRL/lpr mice. J Neuroimmunol. 2009; 207:45–56. https://doi.org/10.1016/j.jneuroim.2008.11.009.
11. Schrott LM, and Crnic LS. Increased anxiety behaviors in autoimmune mice. Behav Neurosci. 1996; 110:492–502. https://doi.org/10.1037//0735-7044.110.3.492.

12. Dubois EL, Horowitz RE, Demopoulos HB, et al. NZB/NZW mice as a model of systemic lupus erythematosus. JAMA. 1966; 195:285–9.
13. Ballok DA. Neuroimmunopathology in a murine model of neuropsychiatric lupus. Brain Res Rev. 2007; 54:67–79. https://doi.org/10.1016/j.brainresrev.2006.12.003.
14. Reeves WH, Lee PY, Weinstein JS, et al. Induction of autoimmunity by pristane and other naturally occurring hydrocarbons. Trends Immunol. 2009; 30:455 – 64. https://doi.org/10.1016/j.it.2009.06.003.
15. Avigan J, and Blumer M. On the origin of pristane in marine organisms. J Lipid Res. 1968; 9:350–2.
16. Zeggar S, Watanabe KS, Teshigawara S, et al. Role of Lgals9 Deficiency in Attenuating Nephritis and Arthritis in BALB/c Mice in a Pristane-Induced Lupus Model. Arthritis Rheumatol. 2018; 70:1089–101. https://doi.org/10.1002/art.40467.
17. Luciano-Jaramillo J, Sandoval-Garcia F, Vazquez-Del Mercado M, et al. Downregulation of hippocampal NR2A/2B subunits related to cognitive impairment in a pristane-induced lupus BALB/c mice. PLoS One. 2019; 14:e0217190. https://doi.org/10.1371/journal.pone.0217190.
18. He YY, Yan Y, Zhang HF, et al. Methyl salicylate 2-O-beta-d-lactoside alleviates the pathological progression of pristane-induced systemic lupus erythematosus-like disease in mice via suppression of inflammatory response and signal transduction. Drug Des Devel Ther. 2016; 10:3183–96. https://doi.org/10.2147/DDDT.S114501.
19. Karnopp TE, Freitas EC, Rieger A, et al. Higher IgG level correlated with vitamin D receptor in the hippocampus of a pristane-induced lupus model. Clin Rheumatol. 2022; 41:1859–66. https://doi.org/10.1007/s10067-022-06094-2.
20. Lin Y, Yan Y, Zhang H, et al. Salvianolic acid A alleviates renal injury in systemic lupus erythematosus induced by pristane in BALB/c mice. Acta Pharm Sin B. 2017; 7:159–66. https://doi.org/10.1016/j.apsb.2016.07.001.
21. Yan Y, Zhang Z, Chen Y, et al. Coptisine Alleviates Pristane-Induced Lupus-Like Disease and Associated Kidney and Cardiovascular Complications in Mice. Front Pharmacol. 2020; 11:929. https://doi.org/10.3389/fphar.2020.00929.
22. Smitka M, Puschmann S, Buschhueter D, et al. Is there a correlation between hippocampus and amygdala volume and olfactory function in healthy subjects? Neuroimage. 2012; 59:1052–7. https://doi.org/10.1016/j.neuroimage.2011.09.024.
23. Arioz BI, Tastan B, Tarakcioglu E, et al. Melatonin Attenuates LPS-Induced Acute Depressive-Like Behaviors and Microglial NLRP3 Inflammasome Activation Through the SIRT1/Nrf2 Pathway. Front Immunol. 2019; 10:1511. https://doi.org/10.3389/fimmu.2019.01511.
24. Gulinello M, and Putterman C. The MRL/lpr mouse strain as a model for neuropsychiatric systemic lupus erythematosus. J Biomed Biotechnol. 2011; 2011:207504. https://doi.org/10.1155/2011/207504.
25. Shoenfeld N, Agmon-Levin N, Flitman-Katzevman I, et al. The sense of smell in systemic lupus erythematosus. Arthritis Rheum. 2009; 60:1484–7. https://doi.org/10.1002/art.24491.

26. Kapadia M, Stanojcic M, Earls AM, et al. Altered olfactory function in the MRL model of CNS lupus. Behav Brain Res. 2012; 234:303–11. https://doi.org/10.1016/j.bbr.2012.07.005.
27. Kapadia M, Zhao H, Ma D, et al. Sustained Immunosuppression Alters Olfactory Function in the MRL Model of CNS Lupus. J Neuroimmune Pharmacol. 2017; 12:555 – 64. https://doi.org/10.1007/s11481-017-9745-6.
28. Moustafa AT, Moazzami M, Engel L, et al. Prevalence and metric of depression and anxiety in systemic lupus erythematosus: A systematic review and meta-analysis. Semin Arthritis Rheum. 2020; 50:84–94. https://doi.org/10.1016/j.semarthrit.2019.06.017.
29. Browne K, Zhang E, Sullivan JK, et al. Lupus-prone B6.Nba2 male and female mice display anti-DWEYS reactivity and a neuropsychiatric phenotype. Brain Behav Immun. 2021; 94:175–84. https://doi.org/10.1016/j.bbi.2021.02.010.
30. Katzav A, Solodeev I, Brodsky O, et al. Induction of autoimmune depression in mice by anti-ribosomal P antibodies via the limbic system. Arthritis Rheum. 2007; 56:938–48. https://doi.org/10.1002/art.22419.
31. Song C, and Leonard BE. The olfactory bulbectomised rat as a model of depression. Neurosci Biobehav Rev. 2005; 29:627 – 47. https://doi.org/10.1016/j.neubiorev.2005.03.010.
32. Santer DM, Yoshio T, Minota S, et al. Potent induction of IFN-alpha and chemokines by autoantibodies in the cerebrospinal fluid of patients with neuropsychiatric lupus. J Immunol. 2009; 182:1192–201. https://doi.org/10.4049/jimmunol.182.2.1192.
33. Yoshio T, Okamoto H, Kurasawa K, et al. IL-6, IL-8, IP-10, MCP-1 and G-CSF are significantly increased in cerebrospinal fluid but not in sera of patients with central neuropsychiatric lupus erythematosus. Lupus. 2016; 25:997–1003. https://doi.org/10.1177/0961203316629556.
34. Fragoso-Loyo H, Richaud-Patin Y, Orozco-Narvaez A, et al. Interleukin-6 and chemokines in the neuropsychiatric manifestations of systemic lupus erythematosus. Arthritis Rheum. 2007; 56:1242–50. https://doi.org/10.1002/art.22451.
35. Alcocer-Varela J, Aleman-Hoey D, and Alarcon-Segovia D. Interleukin-1 and interleukin-6 activities are increased in the cerebrospinal fluid of patients with CNS lupus erythematosus and correlate with local late T-cell activation markers. Lupus. 1992; 1:111–7. https://doi.org/10.1177/096120339200100209.
36. Sakic B, Szechtman H, Braciak T, et al. Reduced preference for sucrose in autoimmune mice: a possible role of interleukin-6. Brain Res Bull. 1997; 44:155 – 65. https://doi.org/10.1016/s0361-9230(97)00107-x.
37. Tonelli LH, Holmes A, and Postolache TT. Intranasal immune challenge induces sex-dependent depressive-like behavior and cytokine expression in the brain. Neuropsychopharmacology. 2008; 33:1038–48. https://doi.org/10.1038/sj.npp.1301488.
38. Wu TH, and Lin CH. IL-6 mediated alterations on immobile behavior of rats in the forced swim test via ERK1/2 activation in specific brain regions. Behav Brain Res. 2008; 193:183–91. https://doi.org/10.1016/j.bbr.2008.05.009.

39. Simen BB, Duman CH, Simen AA, et al. TNFalpha signaling in depression and anxiety: behavioral consequences of individual receptor targeting. Biol Psychiatry. 2006; 59:775 – 85. https://doi.org/10.1016/j.biopsych.2005.10.013.
40. Chourbaji S, Urani A, Inta I, et al. IL-6 knockout mice exhibit resistance to stress-induced development of depression-like behaviors. Neurobiol Dis. 2006; 23:587–94. https://doi.org/10.1016/j.nbd.2006.05.001.
41. Calvani N, Caricchio R, Tucci M, et al. Induction of apoptosis by the hydrocarbon oil pristane: implications for pristane-induced lupus. J Immunol. 2005; 175:4777–82. https://doi.org/10.4049/jimmunol.175.7.4777.
42. Dantzer R. Cytokine, sickness behavior, and depression. Immunol Allergy Clin North Am. 2009; 29:247–64. https://doi.org/10.1016/j.iac.2009.02.002.
43. Veldhuis WB, Floris S, van der Meide PH, et al. Interferon-beta prevents cytokine-induced neutrophil infiltration and attenuates blood-brain barrier disruption. J Cereb Blood Flow Metab. 2003; 23:1060–9. https://doi.org/10.1097/01.WCB.0000080701.47016.24.
44. Saija A, Princi P, Lanza M, et al. Systemic cytokine administration can affect blood-brain barrier permeability in the rat. Life Sci. 1995; 56:775–84. https://doi.org/10.1016/0024-3205(95)00008-t.
45. Kivity S, Agmon-Levin N, Zandman-Goddard G, et al. Neuropsychiatric lupus: a mosaic of clinical presentations. BMC Med. 2015; 13:43. https://doi.org/10.1186/s12916-015-0269-8.
46. Wen J, Xia Y, Stock A, et al. Neuropsychiatric disease in murine lupus is dependent on the TWEAK/Fn14 pathway. J Autoimmun. 2013; 43:44–54. https://doi.org/10.1016/j.jaut.2013.03.002.
47. Minhas U, Minz R, Das P, et al. Therapeutic effect of Withania somnifera on pristane-induced model of SLE. Inflammopharmacology. 2012; 20:195–205. https://doi.org/10.1007/s10787-011-0102-8.
48. Suss P, Hoffmann A, Rothe T, et al. Chronic Peripheral Inflammation Causes a Region-Specific Myeloid Response in the Central Nervous System. Cell Rep. 2020; 30:4082-95 e6. https://doi.org/10.1016/j.celrep.2020.02.109.
49. Diamond B. Antibodies and the Brain: Lessons from Lupus. J Immunol. 2010; 185:2637–40. https://doi.org/10.4049/jimmunol.1090080.
50. Lapteva L, Nowak M, Yarboro CH, et al. Anti-N-methyl-D-aspartate receptor antibodies, cognitive dysfunction, and depression in systemic lupus erythematosus. Arthritis Rheum. 2006; 54:2505–14. https://doi.org/10.1002/art.22031.
51. Kong X, Zhang Z, Fu T, et al. TNF-alpha regulates microglial activation via the NF-kappaB signaling pathway in systemic lupus erythematosus with depression. Int J Biol Macromol. 2019; 125:892–900. https://doi.org/10.1016/j.ijbiomac.2018.12.146.
52. Haruwaka K, Ikegami A, Tachibana Y, et al. Dual microglia effects on blood brain barrier permeability induced by systemic inflammation. Nat Commun. 2019; 10:5816. https://doi.org/10.1038/s41467-019-13812-z.
53. Mike EV, Makinde HM, Der E, et al. Neuropsychiatric Systemic Lupus Erythematosus Is Dependent on Sphingosine-1-Phosphate Signaling. Front Immunol. 2018; 9:2189.

https://doi.org/10.3389/fimmu.2018.02189.

54. Volonte C, Amadio S, Fabbrizio P, et al. Functional microglia neurotransmitters in amyotrophic lateral sclerosis. Semin Cell Dev Biol. 2019; 94:121–8. https://doi.org/10.1016/j.semcdb.2019.04.014.
55. Nayak D, Roth TL, and McGavern DB. Microglia development and function. Annu Rev Immunol. 2014; 32:367–402. https://doi.org/10.1146/annurev-immunol-032713-120240.
56. Kreisel T, Frank MG, Licht T, et al. Dynamic microglial alterations underlie stress-induced depressive-like behavior and suppressed neurogenesis. Mol Psychiatry. 2014; 19:699–709. https://doi.org/10.1038/mp.2013.155.
57. Lu L, Wang H, Liu X, et al. Pyruvate kinase isoform M2 impairs cognition in systemic lupus erythematosus by promoting microglial synaptic pruning via the beta-catenin signaling pathway. J Neuroinflammation. 2021; 18:229. https://doi.org/10.1186/s12974-021-02279-9.
58. Khakh BS. Astrocyte-Neuron Interactions in the Striatum: Insights on Identity, Form, and Function. Trends Neurosci. 2019; 42:617 – 30. https://doi.org/10.1016/j.tins.2019.06.003.
59. Ridet JL, Malhotra SK, Privat A, et al. Reactive astrocytes: cellular and molecular cues to biological function. Trends Neurosci. 1997; 20:570–7. https://doi.org/10.1016/s0166-2236(97)01139-9.
60. Brooks WM, Sibbitt WL, Jr., Kornfeld M, et al. The histopathologic associates of neurometabolite abnormalities in fatal neuropsychiatric systemic lupus erythematosus. Arthritis Rheum. 2010; 62:2055–63. https://doi.org/10.1002/art.27458.
61. Sanmarco LM, Polonio CM, Wheeler MA, et al. Functional immune cell-astrocyte interactions. J Exp Med. 2021; 218. https://doi.org/10.1084/jem.20202715.
62. Wilton DK, Dissing-Olesen L, and Stevens B. Neuron-Glia Signaling in Synapse Elimination. Annu Rev Neurosci. 2019; 42:107 – 27. https://doi.org/10.1146/annurev-neuro-070918-050306.
63. Wellings TP, Brichta AM, and Lim R. Altered neurofilament protein expression in the lateral vestibular nucleus in Parkinson's disease. Exp Brain Res. 2017; 235:3695 – 708. https://doi.org/10.1007/s00221-017-5092-3.
64. Hebbar S, Khandelwal A, Jayashree R, et al. Lipid metabolic perturbation is an early-onset phenotype in adult spinster mutants: a Drosophila model for lysosomal storage disorders. Mol Biol Cell. 2017; 28:3728–40. https://doi.org/10.1091/mbc.E16-09-0674.
65. Grune T, Jung T, Merker K, et al. Decreased proteolysis caused by protein aggregates, inclusion bodies, plaques, lipofuscin, ceroid, and 'aggresomes' during oxidative stress, aging, and disease. Int J Biochem Cell Biol. 2004; 36:2519–30. https://doi.org/10.1016/j.biocel.2004.04.020.
66. Keller JN, Dimayuga E, Chen Q, et al. Autophagy, proteasomes, lipofuscin, and oxidative stress in the aging brain. Int J Biochem Cell Biol. 2004; 36:2376–91. https://doi.org/10.1016/j.biocel.2004.05.003.
67. Riga D, Riga S, Halalau F, et al. Brain lipopigment accumulation in normal and pathological aging. Ann N Y Acad Sci. 2006; 1067:158–63. https://doi.org/10.1196/annals.1354.019.

68. Moreno-Garcia A, Kun A, Calero O, et al. An Overview of the Role of Lipofuscin in Age-Related Neurodegeneration. Front Neurosci. 2018; 12:464. https://doi.org/10.3389/fnins.2018.00464.
69. Saito Y, Miyajima M, Yamamoto S, et al. Accumulation of Senescent Neural Cells in Murine Lupus With Depression-Like Behavior. Front Immunol. 2021; 12:692321. https://doi.org/10.3389/fimmu.2021.692321.
70. Satoh M, and Reeves WH. Induction of lupus-associated autoantibodies in BALB/c mice by intraperitoneal injection of pristane. J Exp Med. 1994; 180:2341–6. https://doi.org/10.1084/jem.180.6.2341.
71. Zhu Y, Ye Y, Zhou C, et al. Effect of Sensory Deprivation of Nasal Respiratory on Behavior of C57BL/6J Mice. Brain Sci. 2021; 11. https://doi.org/10.3390/brainsci11121626.
72. Stover KR, Campbell MA, Van Winssen CM, et al. Early detection of cognitive deficits in the 3xTg-AD mouse model of Alzheimer's disease. Behav Brain Res. 2015; 289:29–38. https://doi.org/10.1016/j.bbr.2015.04.012.
73. Zhang LQ, Zhang W, Li T, et al. GLP-1R activation ameliorated novel-object recognition memory dysfunction via regulating hippocampal AMPK/NF-kappaB pathway in neuropathic pain mice. Neurobiol Learn Mem. 2021; 182:107463. https://doi.org/10.1016/j.nlm.2021.107463.
74. Hisaoka T, Komori T, Kitamura T, et al. Abnormal behaviours relevant to neurodevelopmental disorders in Kirrel3-knockout mice. Sci Rep. 2018; 8:1408. https://doi.org/10.1038/s41598-018-19844-7.
75. Nakamoto C, Kawamura M, Nakatsukasa E, et al. GluD1 knockout mice with a pure C57BL/6N background show impaired fear memory, social interaction, and enhanced depressive-like behavior. PLoS One. 2020; 15:e0229288. https://doi.org/10.1371/journal.pone.0229288.
76. Zhang M, Ballard ME, Kohlhaas KL, et al. Effect of dopamine D3 antagonists on PPI in DBA/2J mice or PPI deficit induced by neonatal ventral hippocampal lesions in rats. Neuropsychopharmacology. 2006; 31:1382–92. https://doi.org/10.1038/sj.npp.1300985.
77. Jordan Walter T, Minassian A, Perry W, et al. Combined prior chronic methamphetamine treatment and gp120 expression reduce PPI in aged male but not female mice. Neurosci Lett. 2022; 780:136639. https://doi.org/10.1016/j.neulet.2022.136639.
78. Srivastava P, Cronin CG, Scranton VL, et al. Neuroprotective and neuro-rehabilitative effects of acute purinergic receptor P2X4 (P2X4R) blockade after ischemic stroke. Exp Neurol. 2020; 329:113308. https://doi.org/10.1016/j.expneurol.2020.113308.

Figures

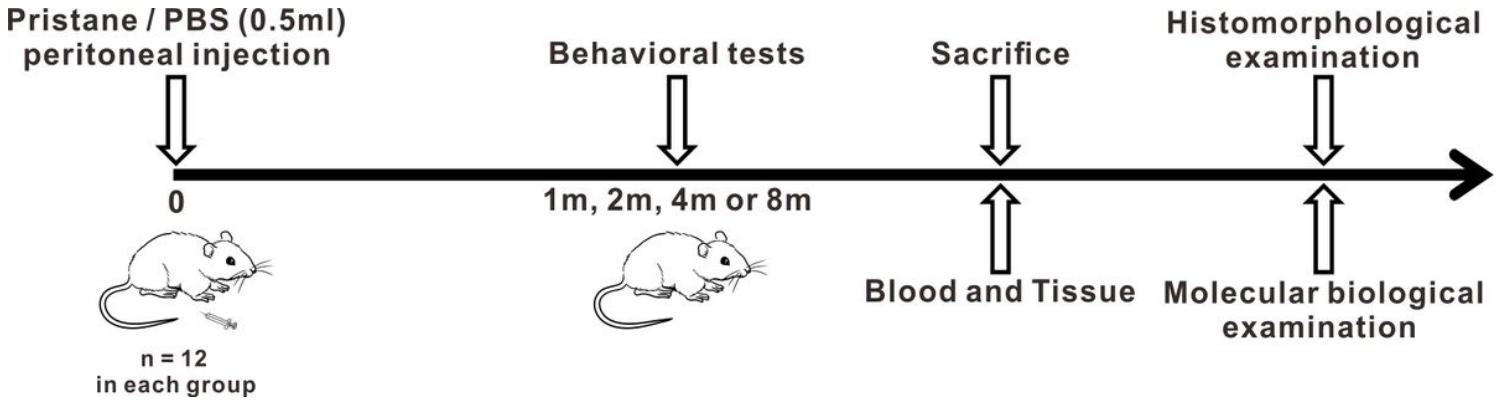

Figure 1

Experimental schedule.

Mice were administered pristane (0.5ml) or PBS via intraperitoneal injection. After conducted a battery of behavioral tests, mice were sacrificed at month 1, 2, 4 or 8. Blood and tissue samples were collected for further histomorphological and molecular biological examinations.

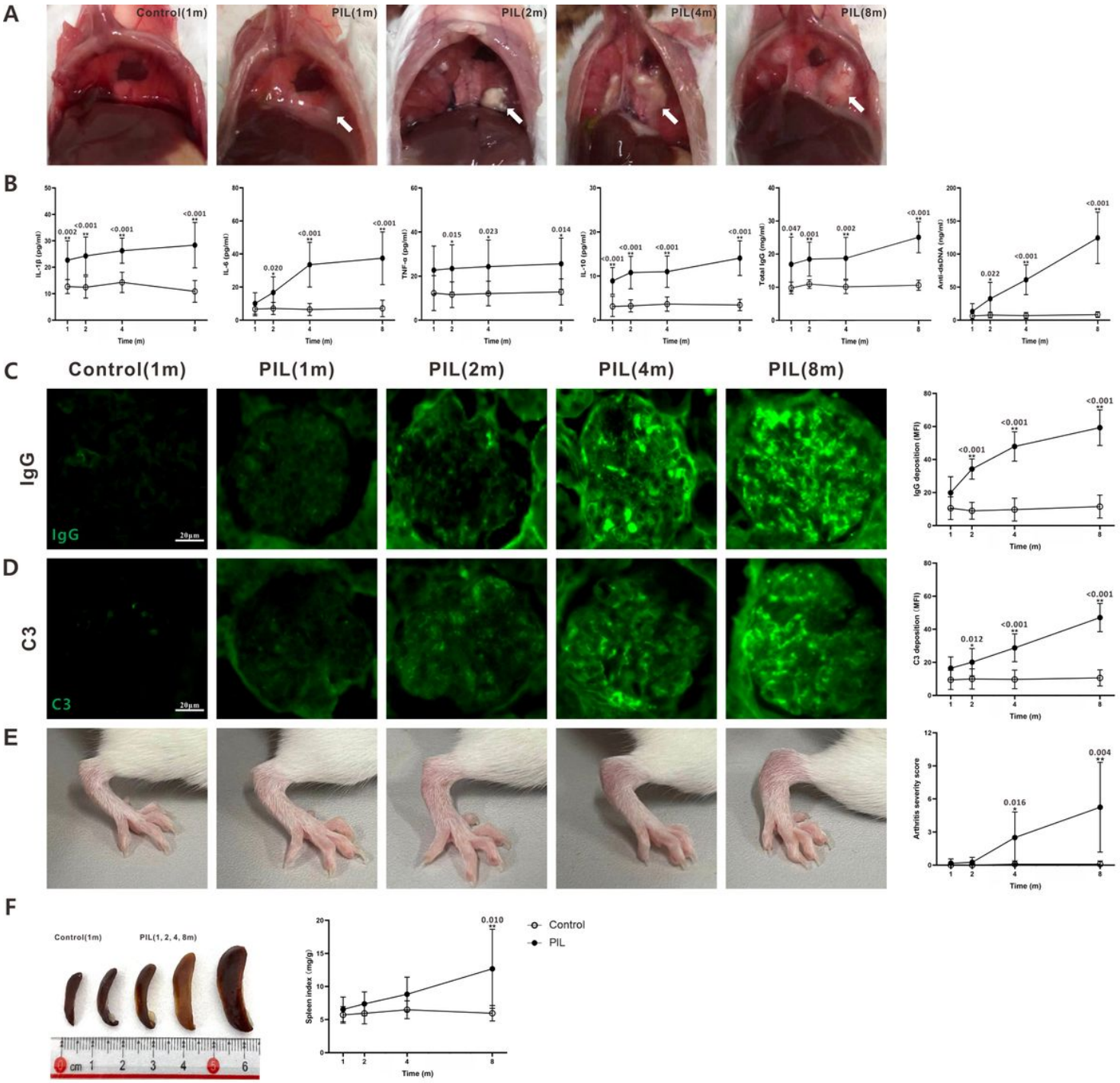

Figure 2

Examination for lupus-like symptoms in PIL mice

(A) Representative images showing lipogranulomas (arrow) adherent to the abdominal surface of the diaphragm in PIL mice. (B) Serum levels of cytokines (IL-1β, IL-6, TNF-α and IL-10), total IgG, and anti-dsDNA, as detected by ELISA. (C) - (D) Representative images of frozen kidney sections stained with IgG and C3, and quantitative analysis of the MFI of IgG and C3 in glomeruli. (E) Representative images of hind paw, and quantitative analysis of arthritis severity score. (F) Representative images of spleen, and

quantitative analysis of spleen index. The data are expressed as the mean ± SEM (n = 12 in each group). Repeated measures ANOVA followed by Tukey's post hoc test: * indicates $p < 0.05$, ** indicates $p < 0.01$.

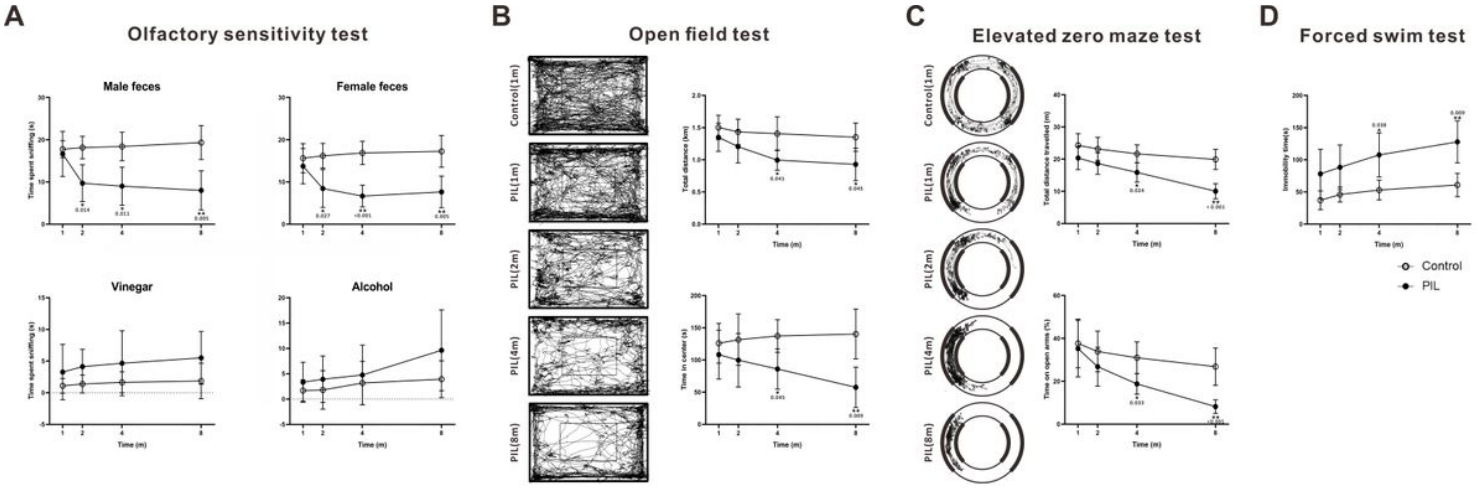

Figure 3

Behavioral assessments of olfactory function and anxiety- and depression-like phenotype

(A) Olfactory sensitivity test. Time spent sniffing male feces, female feces, vinegar and alcohol. (B) Open field test. Left panel showing representative images of the traveling path. Right panel showing quantitative analysis of the total distance travelled and time spent in center. (C) Elevated zero maze test. Left panel showing representative images of the traveling path. Right panel showing quantitative analysis of the total distance travelled and time spent on open arms (%). (D) Forced swim test. Quantitative analysis of immobility time. The data are expressed as the mean ± SEM (n = 12 in each group). Repeated measures ANOVA followed by Tukey's post hoc test: * indicates $p < 0.05$, ** indicates $p < 0.01$.

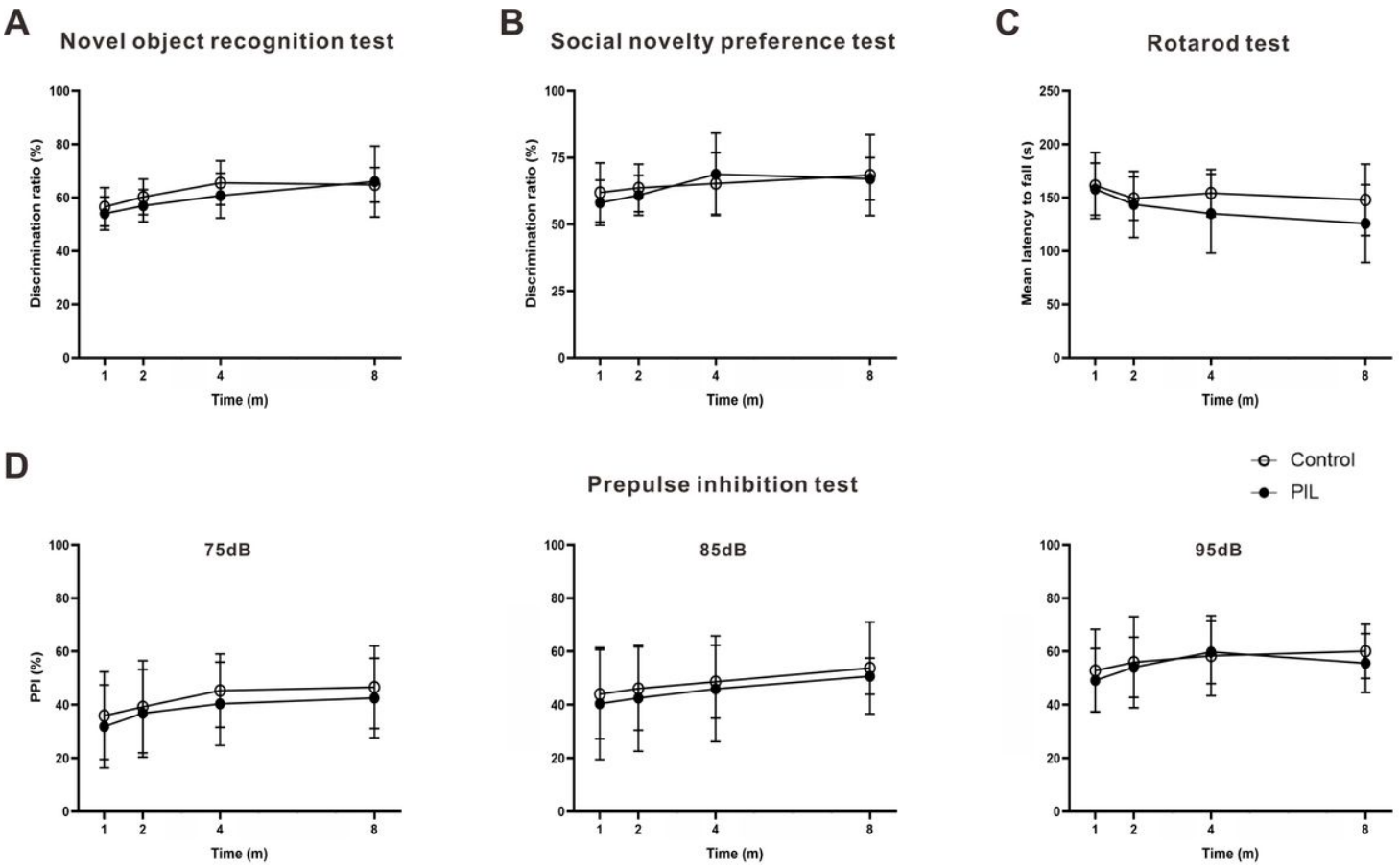

Figure 4

Behavioral assessments of novel object recognition, social novelty preference, rotarod and PPI tests

(A) Novel object recognition test. Quantitative analysis of discrimination ratio. (B) Social novelty preference test. Quantitative analysis of discrimination ratio. (C) Rotarod test. Quantitative analysis of mean latency to fall. (D) Quantitative analysis of PPI% on 75dB, 85dB or 95dB. The data are expressed as the mean ± SEM (n = 12 in each group). Repeated measures ANOVA followed by Tukey's post hoc test.

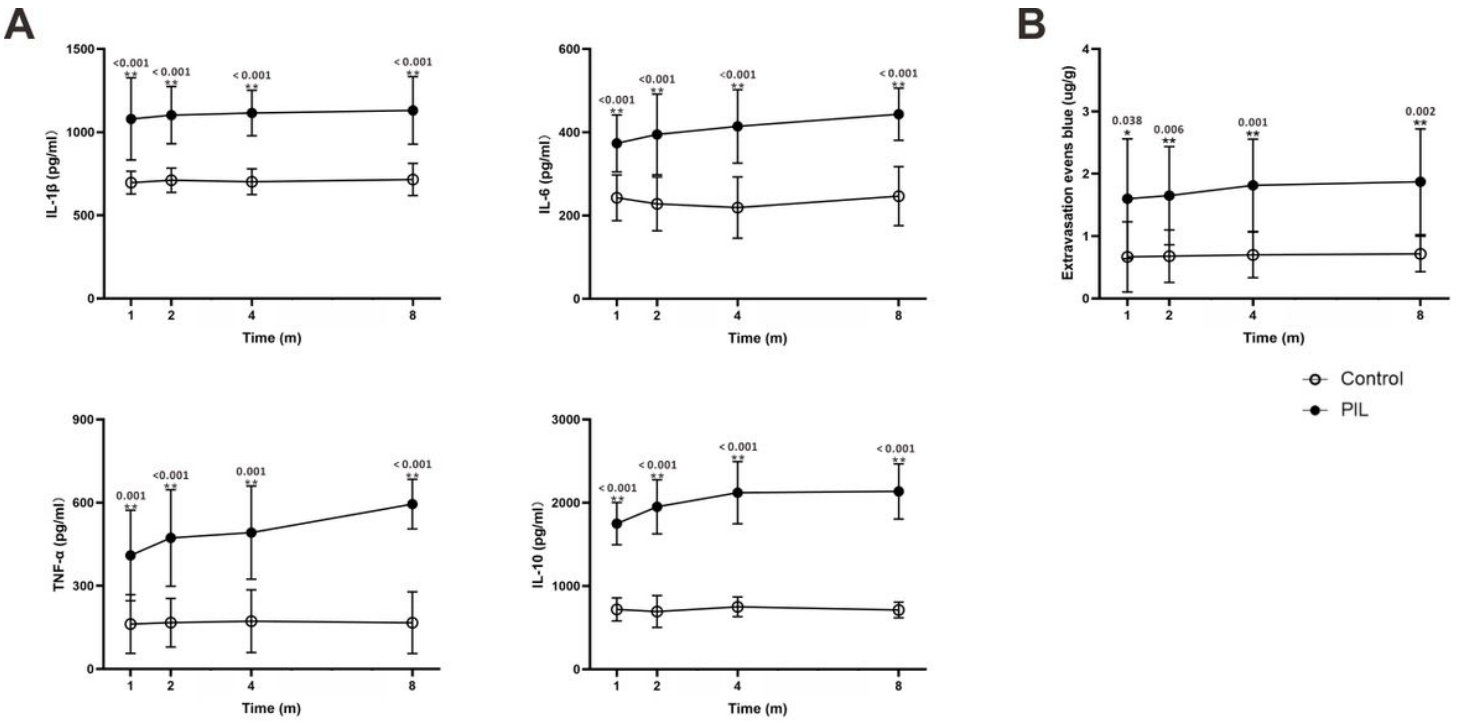

Figure 5

Levels of brain cytokines and BBB permeability

(A) Brain levels of cytokines (IL-1β, IL-6, TNF-α and IL-10), as detected by ELISA. (B) Quantitative analysis of evens blue dye extravasation. The data are expressed as the mean ± SEM (n = 12 in each group). Repeated measures ANOVA followed by Tukey's post hoc test: * indicates $p < 0.05$, ** indicates $p < 0.01$.

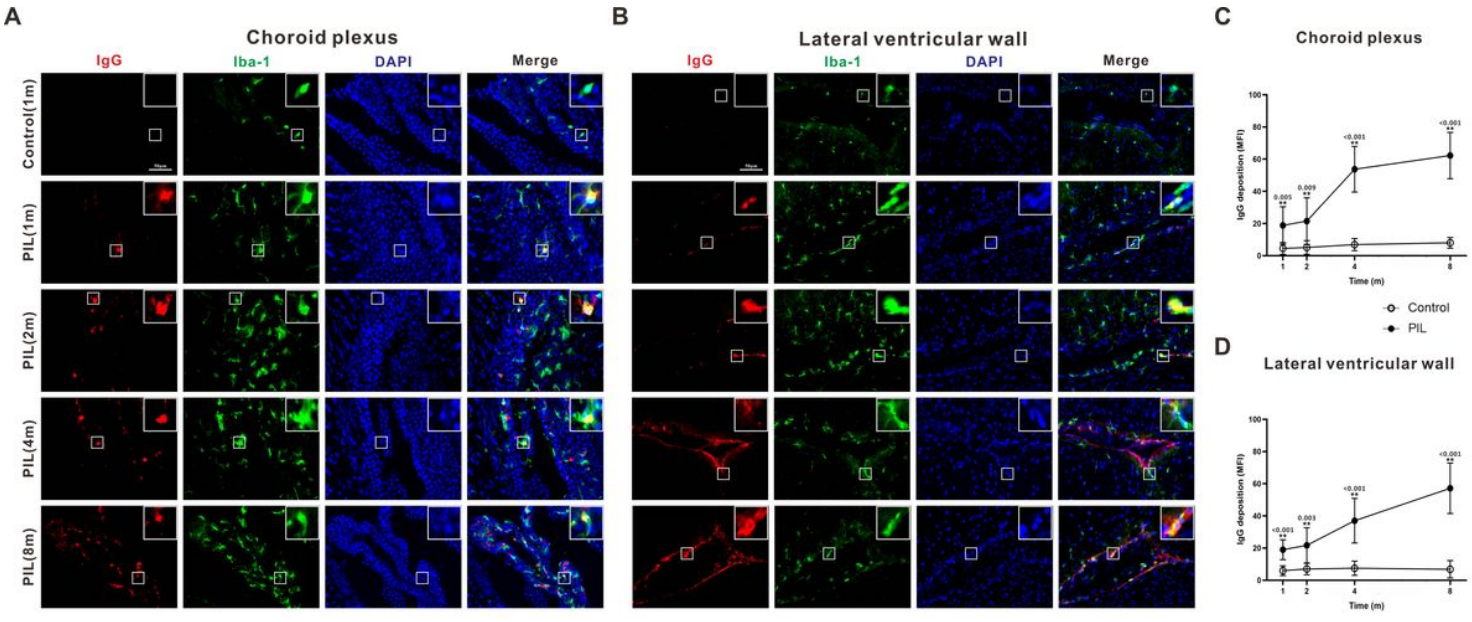

Figure 6

Examination for IgG deposition in the choroid plexus and lateral ventricular wall

(A) - (B) Representative images of IgG deposition in the choroid plexus and lateral ventricular wall. White square showing the co-localization of an enlarged Iba-1-immunoreactive microglia (green) and IgG (red). (C) - (D) Quantitative analysis of IgG deposition in the choroid plexus and lateral ventricular wall by MFI. DAPI staining to locate nuclei with the blue fluorescence. The data are expressed as the mean ± SEM (n = 12 in each group). Repeated measures ANOVA followed by Tukey's post hoc test: ** indicates $p < 0.01$.

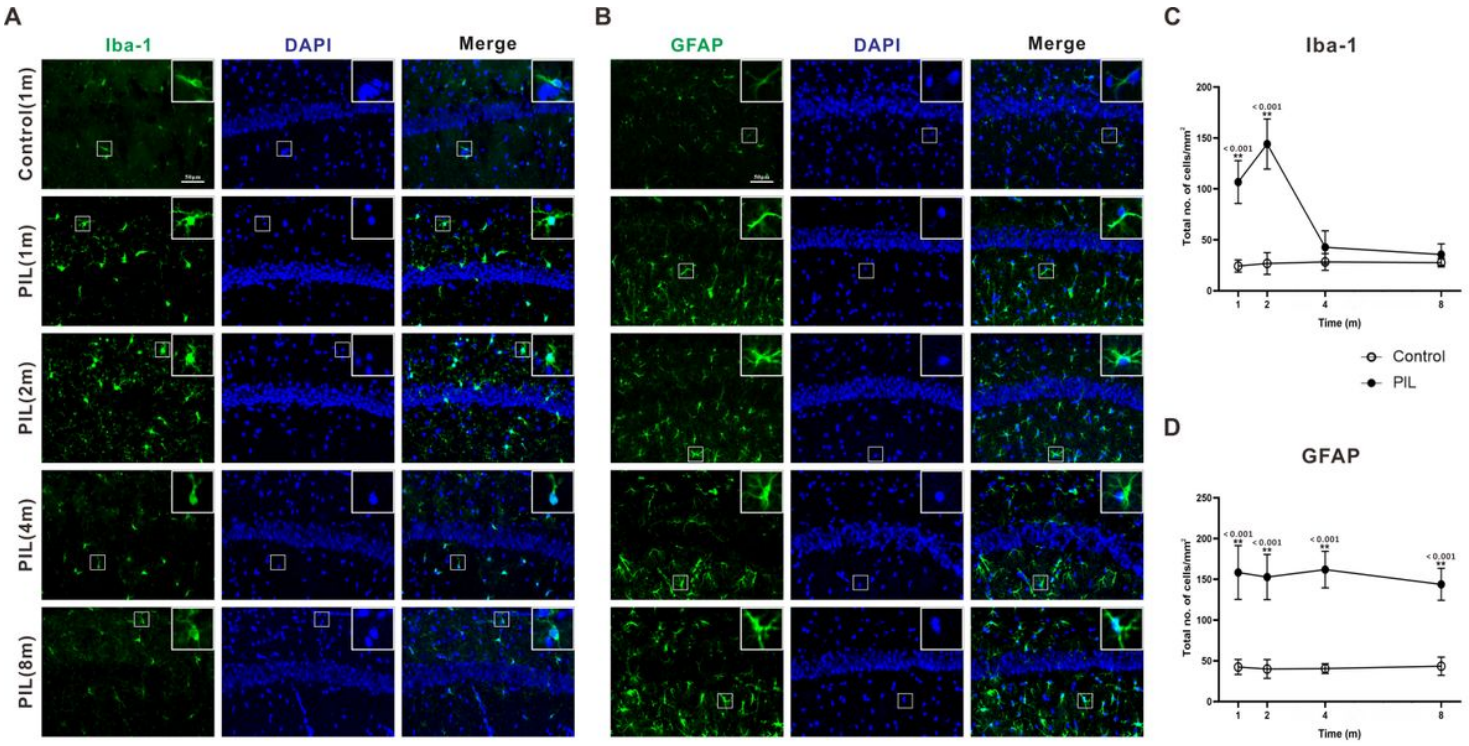

Figure 7

Density and morphology of microglia and astrocytes in the hippocampus

(A) - (B) Representative images showing Iba-1-immunoreactive microglia and GFAP-immunoreactive astrocytes in the hippocampus. DAPI staining to locate nuclei with the blue fluorescence. White square showing an enlarged cell to compare the morphology. (C) - (D): Quantitative analysis of the density of Iba-1- and GFAP- immunoreactive cells. The data are expressed as the mean ± SEM (n = 12 in each group). Repeated measures ANOVA followed by Tukey's post hoc test: ** indicates $p < 0.01$.

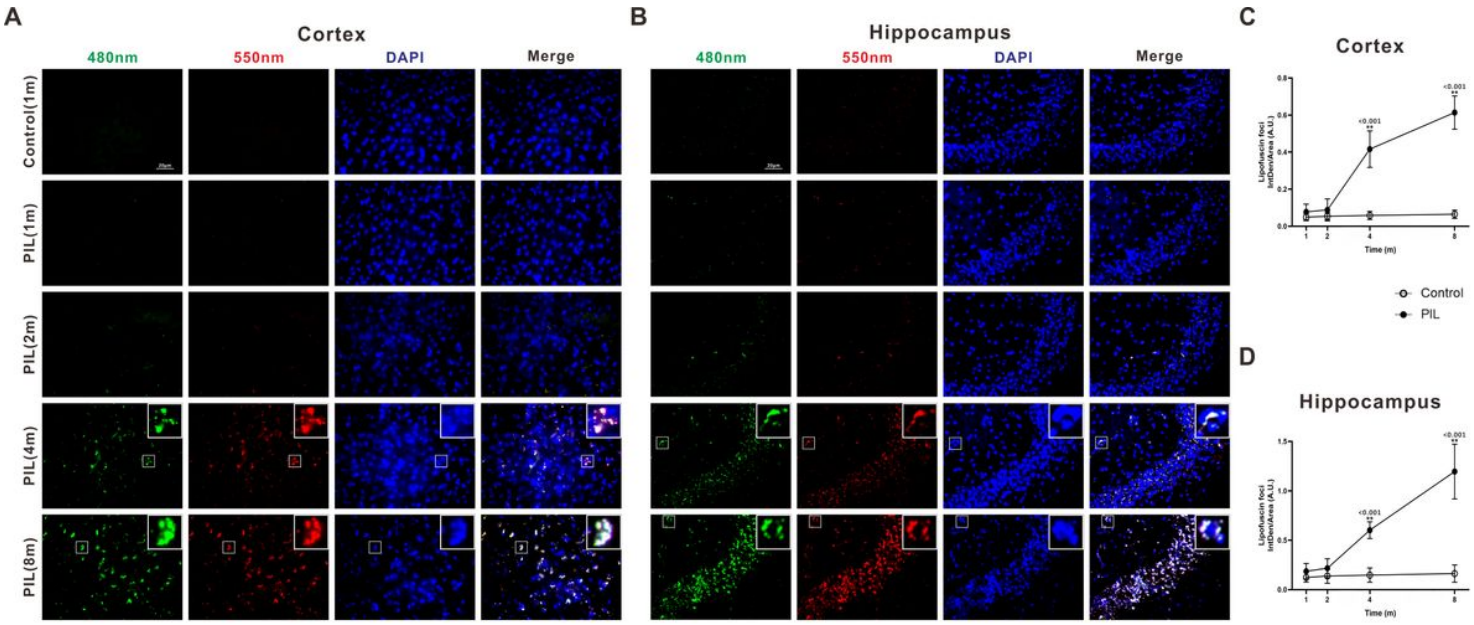

Figure 8

Examination for lipofuscin deposition in the cortex and hippocampus

(A) - (B) Representative images showing autofluorescent lipofuscin at 480nm (green) and 550nm (red) exciting light in the cortex and hippocampus. DAPI staining to locate nuclei with the blue fluorescence. White square showing the co-localization of an enlarged neuron (blue) with autofluorescences (green and red). (C) - (D) Quantification analysis of lipofuscin foci in the cortex and hippocampus. The data are expressed as the mean ± SEM (n = 12 in each group). Repeated measures ANOVA followed by Tukey's post hoc test: ** indicates $p < 0.01$.